



Article

Design and Simulation of Air-Breathing Micro Direct Methanol Fuel Cells with Different Anode Flow Fields

Huichao Deng ¹, Jiaxu Zhou ^{1,*} and Yufeng Zhang ²

¹ School of Mechanical Engineering and Automation, Beihang University, Beijing 100191, China; denghuichao@buaa.edu.cn

² MEMS Center, Harbin Institute of Technology, Harbin 150001, China; yufeng_zhang@hit.edu.cn

* Correspondence: Jiaxuzhou@buaa.edu.cn; Tel.: +86-010-8233-9055

Abstract: The design of the anode flow field is critical for yielding better performance of micro direct methanol fuel cells (μ DMFCs). In this work, the effect of different flow fields on cell performance was investigated by the simulation method. Compared with grid, parallel and double-serpentine flow fields, a single-serpentine flow field can better improve the mass transfer efficiency of methanol and the emission efficiency of the carbon dioxide by-product. The opening ratio and channel length also have important effects on the cell performance. The cells were manufactured using silicon-based micro-electro-mechanical system (MEMS) technologies and tested to verify the simulation results. The experimental results show that the single-serpentine flow field represents a higher peak power density (16.83 mWcm^{-2}) than other flow fields. Moreover, the results show that an open ratio of 47.3% and a channel length of 63.5 μm are the optimal parameters for the single-serpentine flow field.

Keywords: micro direct methanol fuel cell; simulation; MEMS; serpentine flow field; mass transport



Citation: Deng, H.; Zhou, J.; Zhang, Y. Design and Simulation of Air-Breathing Micro Direct Methanol Fuel Cells with Different Anode Flow Fields. *Micromachines* **2021**, *12*, 253. <https://doi.org/10.3390/mi12030253>

Academic Editor: Jin-yuan Qian

Received: 6 February 2021
Accepted: 25 February 2021
Published: 2 March 2021

Publisher's Note: MDPI stays neutral with regard to jurisdictional claims in published maps and institutional affiliations.



Copyright: © 2021 by the authors. Licensee MDPI, Basel, Switzerland. This article is an open access article distributed under the terms and conditions of the Creative Commons Attribution (CC BY) license (<https://creativecommons.org/licenses/by/4.0/>).

1. Introduction

Micro direct methanol fuel cells (μ DMFCs) have attracted much attention in portable and mobile electronic products such as notebook computers and mobile phones due to their high efficiency, high energy density, room-temperature operation and simple structure [1–6]. The current collector, as a major component of μ DMFCs, is responsible for transport of reactants, structural support for membrane electrode assembly (MEA) and current collection. Therefore, the design of an anode flow field on the current collector is a critical factor for increasing μ DMFCs performance [7,8].

Many efforts have focused on improving the cell performance by changing the anode flow field design. Flow field parameter optimization and new pattern design were considered to be effective methods to improve cell performance. The open ratios (ratio of perforation area to current collector area) and channel size (channel length, width and depth) have been shown to be the key factors that influence the cell performance. The effects of channel patterns and open ratios (ratio of perforation area to current collector area) on the performance of passive μ DMFCs were investigated by experiments and simulations in [9]. Results indicate that the vertical stripe pattern (VSP) is preferred for anodes, and the best performance had an open ratio of 45.6%. The open ratios of the anode and cathode current collectors on the power density of passive μ DMFCs were also studied in [10]. The best output (3.14 mWcm^{-2}) was scored with a lower open ratio (34%) on both sides with a methanol concentration of 2 M. The behavior of the micro-scale effect in μ DMFCs was investigated through both simulations and experiments. The maximum power density (27.1 mWcm^{-2}) was scored at the optimal feature size of 0.6 mm and the aspect ratio of 2:1 [11]. In addition, the channel cross-sectional flow field was optimized experimentally. A passive micro direct methanol fuel cell was fabricated with both rectangular and trapezoidal cross-sectional geometry at the anode and cathode using the micro-electro-mechanical system (MEMS) technology fabrication technique. According

to results from [12], the power density (6.64 mWcm^{-2}) of trapezoidal cross-section channels was nearly two times higher than the power density (3.9 mWcm^{-2}) of rectangular cross-section channels at a 7 M methanol concentration. A serpentine channel with a non-uniform cross-section was designed and analyzed in [13]. Numerical results show that non-uniform converging designs enhance the peak power generation performance by as much as 12% at high-current-density operations. In order to improve the performance of μDMFCs , a series of new pattern designs were proposed along with optimization of the flow field parameters [14–19].

Parameter optimization and new pattern design anode flow fields have great effects on the performance of μDMFCs . Different flow fields result in different pressure distributions. The pressure difference between adjacent flow channels of the ribs affects the convection and diffusion of methanol in the diffusion layer, changes the distribution of methanol, and affects the performance of μDMFCs . In addition, the pressure difference increases the mass transfer rate of methanol molecules and covers the emission of carbon dioxide. Based on the above considerations, we investigated different anode flow fields of self-breathing μDMFCs . The model with different flow fields was built to analyze the effect of flow field parameters on the performance of μDMFCs . The simulation results show that the single serpentine design gave a better performance and open ratios and channel lengths affect the anode flow field structure. Meanwhile, the silicon-based self-breathing μDMFCs were fabricated to verify the simulation results by MEMS technology. The experimental results agree well with the simulation results.

2. Computational Model

2.1. Flow Field Design

This paper mainly considers the influence of the anode flow field on cell performance. Therefore, the cathode current collectors are perforated collectors with the same structure. To investigate the effects of anode flow field configurations on the cell performance at the same conditions, four types of flow fields including grid, parallel, single-serpentine and double-serpentine flow field were designed with approximately the same active area and open ratio as shown in Figure 1. The active area and open ratio were set to around 64 mm^2 and 73.0%, respectively. Other structure parameters are shown in Table 1.

Table 1. Geometric parameters of four types of flow fields.

| Type of Flow Field | Effective Width (mm) | Channel Depth (mm) | Ridge Width (mm) | Effective Area (mm × mm) | Open Ratio (%) |
|------------------------------|----------------------|--------------------|------------------|--------------------------|----------------|
| Grid flow field | 0.55 | 0.24 | 0.69 | 7.99×7.99 | 72.9 |
| Parallel flow field | 0.75 | 0.24 | 0.45 | 7.95×7.95 | 72.9 |
| Single-serpentine flow field | 0.8 | 0.24 | 0.4 | 8.0×8.0 | 73.0 |
| Double-serpentine flow field | 0.575 | 0.24 | 0.25 | 8.0×8.0 | 73.6 |

For single-serpentine flow fields, the influence of channel open ratios on cell performance was analyzed by variations of the channel and support ridge widths. The respective open ratios of the four types of single-serpentine flow fields with the same active areas were 29.1%, 47.3%, 60.6% and 73.0%, and other parameters are shown in Table 2.

In addition, four single-serpentine flow fields with different channel lengths and the same open ratios (47.3–47.8%) were designed to study the effects of channel lengths on cell performance, as shown in Table 3. The four channel lengths (47.32, 63.50, 79.60 and 96.03 mm) were realized by modifying the channel widths and the channel numbers (5, 7, 9 and 11).

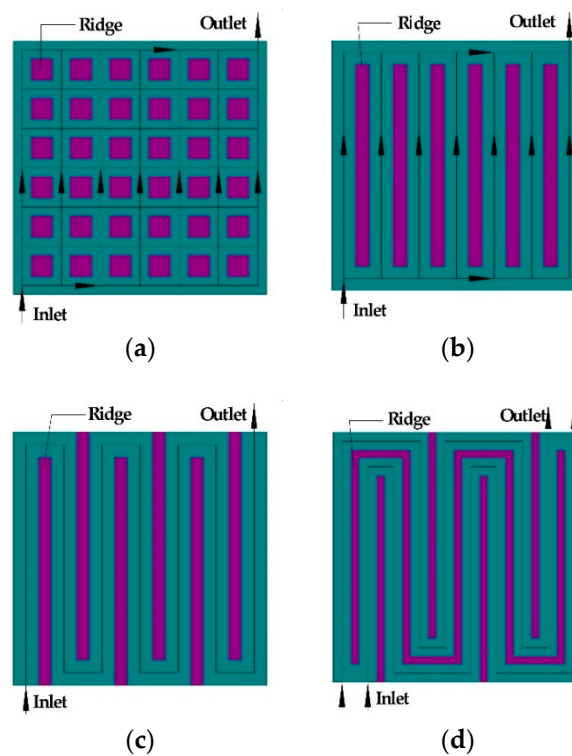


Figure 1. Design of the anode flow fields: (a) grid flow fields, (b) parallel flow fields, (c) single-serpentine flow fields, and (d) double-serpentine flow fields.

Table 2. Geometric parameters of the single-serpentine flow fields with four open ratios.

| Open Ratio (%) | Width of Channel (mm) | Channel Depth (mm) | Width of Ridge (mm) | Length of Channel (mm) | Active Area (mm × mm) |
|----------------|-----------------------|--------------------|---------------------|------------------------|-----------------------|
| 29.1 | 0.3 | 0.24 | 0.98 | 63.68 | 7.98 × 7.98 |
| 47.3 | 0.5 | 0.24 | 0.75 | 63.50 | 8.0 × 8.0 |
| 60.6 | 0.65 | 0.24 | 0.57 | 63.32 | 7.97 × 7.97 |
| 73.0 | 0.8 | 0.24 | 0.4 | 63.20 | 8.0 × 8.0 |

Table 3. Geometric parameters of the single-serpentine flow fields with four channel lengths.

| Length of Channel (mm) | Width of Channel (mm) | Depth of Channel (mm) | Width of Ridge (mm) | Open Ratio (%) | Effective Size (mm × mm) |
|------------------------|-----------------------|-----------------------|---------------------|----------------|--------------------------|
| 47.32 | 0.68 | 0.24 | 1.15 | 47.4 | 8.0 × 8.0 |
| 63.50 | 0.5 | 0.24 | 0.75 | 47.3 | 8.0 × 8.0 |
| 79.60 | 0.4 | 0.24 | 0.55 | 47.8 | 8.0 × 8.0 |
| 96.03 | 0.33 | 0.24 | 0.44 | 47.5 | 8.03 × 8.03 |

2.2. Model Description and Assumption

Two factors have significant direct effects on the cell performance for the anode of μ DMFCs. Firstly, the speed of methanol mass transport in the diffusion layer impacts the process and efficiency of the electrochemical reaction. Secondly, CO_2 blocking in the anode negatively influences the methanol mass transport. Therefore, efforts to design the anode flow fields will contribute to improving the cell performance. Thus, we built a three-dimensional steady-state multi-field coupled model for the anode of μ DMFCs to investigate the mass transport, including anode flow channels, an anode diffusion layer

and an anode catalyst layer. Several assumptions for simplification are introduced in this model:

- (1) All processes in the μ DMFCs are under steady-state conditions.
- (2) The average hole transfer model is applied in the diffusion layer.
- (3) The catalyst layer is simplified as a plane without thickness.
- (4) The CO_2 generated at the anode dissolves in water completely, and its influence is ignored.
- (5) The methanol density in the anode flow channel is considered as a constant and it belongs to the incompressible flow.
- (6) The influence of gravity is ignored.

2.3. Governing Equations

(1) Navier–Stokes (N-S) Equation

The momentum transfer of the fluid in the flow channel can be described by the Navier–Stokes (N-S) equation. The influence of CO_2 can be ignored because the methanol density in the anode flow channel can be considered as a constant. The flow of the methanol in the flow channels is considered to be laminar flow and it is continuous. The momentum of the flow comes from the pressure difference ∇p . The N-S equation can be expressed as follows:

$$\rho \frac{\partial \mathbf{u}}{\partial t} + (\rho \mathbf{u} \cdot \nabla) \mathbf{u} = -\nabla p + \nabla \cdot \boldsymbol{\tau} + F, \quad (1)$$

$$\nabla \cdot \mathbf{u} = 0, \quad (2)$$

$$\boldsymbol{\tau} = \eta \left(\nabla \mathbf{u} + (\nabla \mathbf{u})^T \right), \quad (3)$$

where ρ is the density of the methanol solution, \mathbf{u} represents the flow velocity of the liquid, p is the liquid pressure, $\boldsymbol{\tau}$ is the liquid viscid pressure tensor, F represents the external force, and η represents the liquid viscosity coefficient.

(2) Diffusion-Convection Equation

In this model, the influence on fluid that is caused by CO_2 is neglected, so the mass transfer within the flow channel only occurs between the methanol and water. The diffusion in the flow channel can be described by Fick's law, and the velocity of the convection can be achieved from the N-S equation. Fick's law can be expressed as follows:

$$-D \nabla c = \mathbf{R}, \quad (4)$$

where D represents the diffusion coefficient of methanol in water, c is the concentration of the methanol, and \mathbf{R} represents the reaction rate. The velocity vector in the flow channel is described by the N-S equation and the velocity vector in the diffusion layer is described by Darcy's law. The mass transfer equation in the flow channel is thus obtained:

$$\nabla \cdot (-D \nabla c) = \mathbf{R} - \mathbf{u} \nabla \cdot c. \quad (5)$$

The diffusion coefficient of methanol in the diffusion layer is

$$D = D_{eff} \cdot (\varepsilon)^{1.5}, \quad (6)$$

$$D_{eff} = D_{ref} \cdot \exp \left(2436 \left(\frac{1}{353} - \frac{1}{T} \right) \right), \quad (7)$$

where D_{ref} is the diffusion coefficient of methanol in water at the temperature of 353.15 K, ε represents the absolute permeability of the porous medium, and T is the working temperature of the fuel cell.

(3) Darcy's Law

In the anode diffusion layer, the momentum of the methanol solution convection comes from the liquid pressure difference and can be described by Darcy's law:

$$\nabla \cdot \left(\rho \left(-\frac{\kappa}{\eta} \nabla p \right) \right) = Q_{darcy}, \quad (8)$$

$$\mathbf{u} = -\frac{\kappa}{\eta} \nabla p, \quad (9)$$

where κ represents the absolute permeability of the porous medium, and Q_{darcy} is the source term.

(4) Ohm's Law

The electron conduction and the distribution of the electron conduction potential in the anode diffusion layer can be described by Ohm's law:

$$\nabla(-\sigma_l \nabla \phi_l) = -S_a \cdot i_a. \quad (10)$$

The proton conduction and the distribution of the electron conduction potential in the anode diffusion layer can be described as

$$\nabla(-\sigma_i \nabla \phi_i) = S_a \cdot i_a, \quad (11)$$

where σ_i is the effective electronic conductivity, ϕ_i is the anode electric potential, S_a represents the surface area, and i_a represents the anode current density.

(5) Butler–Volmer (B-V) Equation

The anode current density generated by the methanol oxidation in the catalyst layer can be described by the B-V equation:

$$i_a = i_0 \cdot \exp\left(0.5F \frac{eta}{(R \cdot T)}\right) \cdot \left(\frac{c}{c_{ref}}\right) \cdot (c \geq 0), \quad (12)$$

where i_0 represents the exchange current density, F is the Faraday constant, eta represents the overvoltage, and c_{ref} is the reference methanol concentration.

2.4. Boundary Conditions

(1) N-S Equation

All the walls in the flow channel are solid except for those of the inlet and outlet, that is to say, the fluid has no movement in the wall. The fluid enters the flow channel at a certain velocity due to the external influence, and the boundary condition for the inlet velocity is

$$\mathbf{n} \cdot \mathbf{u} = u_0, \quad (13)$$

where u_0 represents the liquid feeding rate. As the outlet is exposed to air, so the pressure at the outlet is set as the standard atmosphere:

$$p = p_0, \quad (14)$$

where p_0 represents the standard atmosphere.

(2) Diffusion-Convection Equation

The methanol flow into the flow channel through the inlet at the concentration of c_0 , and the boundary condition at the inlet is

$$c = c_0. \quad (15)$$

As the concentration of the methanol is uncertain, it is set as the convection flux, which means the diffusion concentration of methanol in the direction of the unit vector is zero. The convection flux is uncertain and its boundary condition is

$$\mathbf{n} \cdot (D \nabla c) = 0. \quad (16)$$

(3) Darcy's Law

The walls are all considered insulated and symmetrical. There is a pressure gradient at the boundary face of the interface of the flow channel and the diffusion layer. This pressure gradient can be expressed as below:

$$\frac{\nabla p}{\nabla x} = \frac{\partial p}{\partial n'}, \quad (17)$$

The velocity is approximately:

$$-\mathbf{n} \cdot \mathbf{u} = \frac{\left(\frac{\kappa}{\eta}\right) \nabla p}{1[\text{mm}]}. \quad (18)$$

(4) B-V Equation

The mass transfer of the methanol in the catalyst layer is a flux:

$$-\mathbf{n} \cdot \mathbf{N} = N_0, \quad (19)$$

$$\mathbf{N} = -D \nabla c + c \mathbf{u}, \quad (20)$$

$$N_0 = -\frac{i_a}{(6 \cdot F)}. \quad (21)$$

(5) Ohm's Law

The internal inward normal current density J_0 at the interface of the diffusion layer and the catalyst layer is set as

$$-\mathbf{n} \cdot \mathbf{J} = J_0 = -i_a. \quad (22)$$

Set the electrical potential energy at the flow channel polar plate as V_{cell} :

$$V = V_{cell}. \quad (23)$$

Other surfaces are considered insulated.

2.5. Solution Procedure

In the study, the above simulation was implemented in COMSOL Multiphysics® 5.5 (COMSOL, Stockholm, Sweden). COMSOL Multiphysics® 5.5 is a multi-physics simulation software using the finite element method. The governing equations and boundary conditions are implemented using built-in modules (Secondary Current Distribution, Transport of Diluted Species and Darcy's Law) and custom functions. A structured hexahedral mesh was generated by swept and mapped methods. The given boundary conditions are inlet velocity and pressure. The default steady-state solver was used to solve the model. Other parameters used in the simulation are given in Table 4.

Table 4. Parameters used in the anode model calculations.

| Parameter Names | Parameter Values |
|---|---|
| Faraday constant (F) | 96,495 C/mol |
| Gas law constant (R) | 8.314 J/(mol·K) |
| Standard value (V_{cell}) | 0.2 V |
| Standard diffusion coefficient of the methanol in the water (D_{ref}) | 6.69×10^{-9} m ² /s |
| Electrical conductivity of the electron (σ) | 10 S/m |
| Density of the methanol solution (ρ) | 1000 kg/m ³ |
| Standard consistence of the methanol (c_{ref}) | 1000 mol/m ³ |
| Exchange current density at the anode (i_0) | 94.25 A/m ² |
| Viscosity coefficient of the methanol solution (η) | 0.9×10^{-3} kg/(m·s) |
| permeability (κ) | 1.2×10^{-12} m ² |
| overvoltage (η) | 0.2 V |
| porosity (ϵ) | 0.6 |
| Working temperature (T) | 293 K |
| Liquid filling rate (u_0) | 1.7×10^{-8} m ³ /s |
| The consistence of methanol (c_0) | 1000 mol/m ³ |
| Atmospheric pressure (p_0) | 1.013×10^5 Pa |
| Specific surface area (S_a) | 10^7 m ⁻¹ |
| Gibbs free energy (G_a) | -166.27×10^3 J/mol |
| Reaction enthalpy (H_a) | -238.66×10^3 J/mol |
| Thermal conductivity (k) | 1.6 W/(m·K) |
| Specific heat capacity at standard pressure (C_p) | 2531 J/(kg·K) |

3. Simulation Results and Discussion

3.1. Analysis of Four Anode Flow Fields

Figure 2 shows the pressure distributions of four anode flow fields. It was clear that the pressure difference of the inlet and outlet decreased in the following sequence: single-serpentine, double-serpentine, parallel, and grid flow fields, which were 74.39, 30.16, 9.58 and 8.74 Pa, respectively, according to the calculation. It was known that the working precondition of μ DMFCs was the methanol flow in anode flow fields. The larger the pressure gradient, the faster and more uniformly the liquid flowed, which was not only propitious to increase the transport efficiency of reactants in the diffusion layer, but also favorable to the exclusion of resultants. In that case, a single-serpentine flow field was the first priority.

Figure 3 illustrates the velocity distributions in four anode flow fields. For the grid flow field and parallel flow field, the flow rate was rather fast at the inlet. However, it had a sharp decrease when the methanol solutions flowed into the channels and stagnant fluid appeared in a large region, which brought an uneven distribution of reactants as well as degradation of flow channel utilization. Furthermore, it had a considerable impact on the exhaust of resultants and heat, which would further cause CO₂ to block the channel and local over-heating. The above factors could absolutely decrease the lifetime and performance of μ DMFCs. However, for single-serpentine and double-serpentine flow fields, the flow rate was even in most of the flow channels, except that there might be a small quantity of stagnancy at the corner of the flow passageway. The respective average flow rates were 0.0094 and 0.0055 m/s, which were more favorable than those of the grid and parallel flow fields.

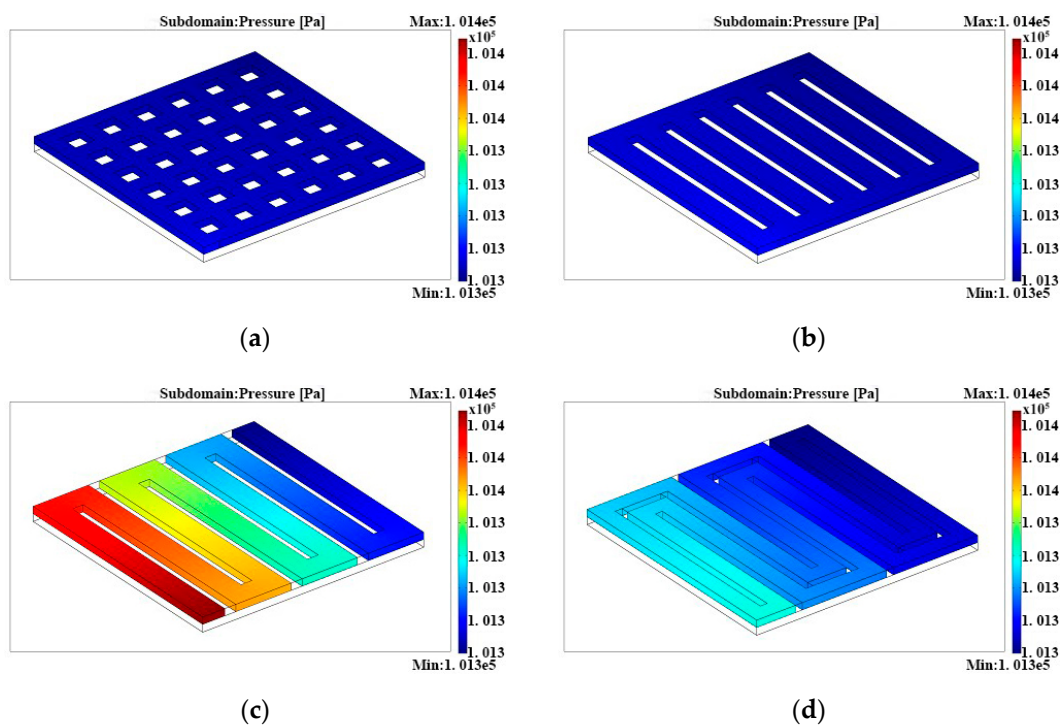


Figure 2. Pressure distributions in (a) grid flow fields, (b) parallel flow fields, (c) single-serpentine flow fields, and (d) double-serpentine flow fields.

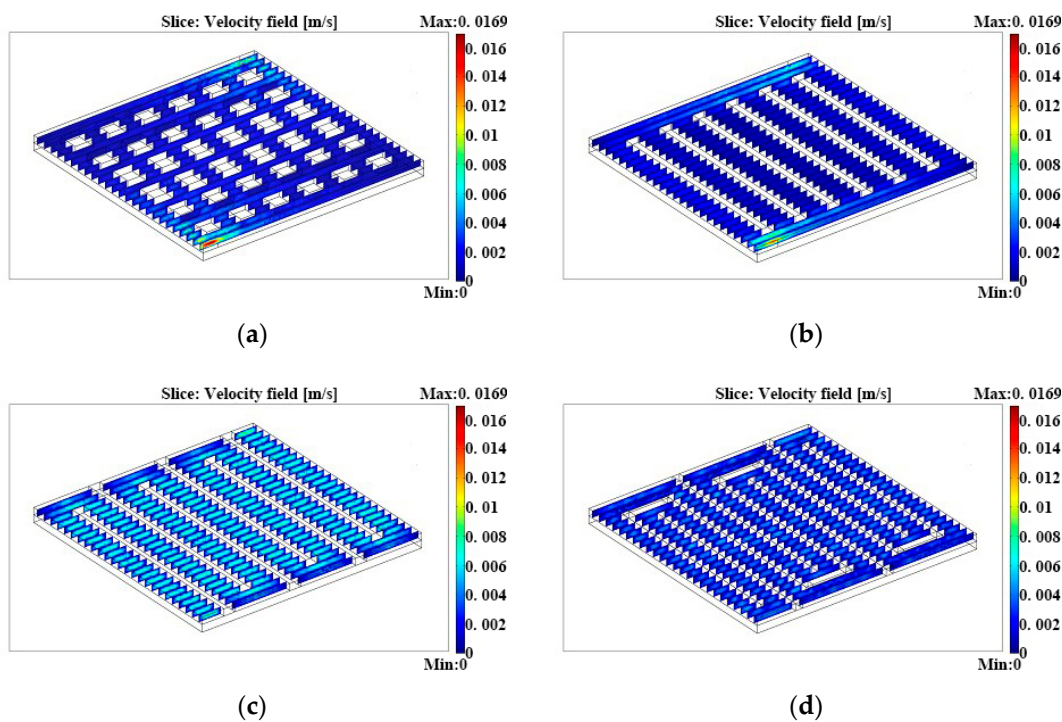


Figure 3. Flow rate distributions in (a) grid flow fields, (b) parallel flow fields, (c) single-serpentine flow fields, and (d) double-serpentine flow fields.

Figure 4 shows the methanol concentration distributions at the catalyst layer for four anode flow fields. Based on the calculation, the respective maximum methanol concentrations were 586.58, 585.29, 602.03 and 590.93 mol/m³, and the respective minimum values

were 353.27, 336.11, 339.04 and 320.35 mol/m³. The single-serpentine flow field could help the catalyst layer obtain the highest methanol concentration that the methanol transport could provide. However, the high pressure of the single-serpentine flow field could also result in the increment of methanol concentration differences. The peak concentrations in the other flow fields were not quite different from each other, and the difference was smallest in the grid flow field. As the diffusion layer directly contacted the support ridge of the flow channels, methanol molecules could enter the bottom of the support ridge by cross motion. Therefore, the methanol concentration in the support ridge, which corresponds to the catalyst layer (the dead mass transport area under the support ridge), was considerably lower than that in the corresponding flow field, which might cause unevenness of concentration distributions. In fact, the methanol molecule transport velocity at the diffusion layer under the support ridge could be enhanced by increasing the pressure difference of neighbor flow channels so that the concentration difference could be reduced.

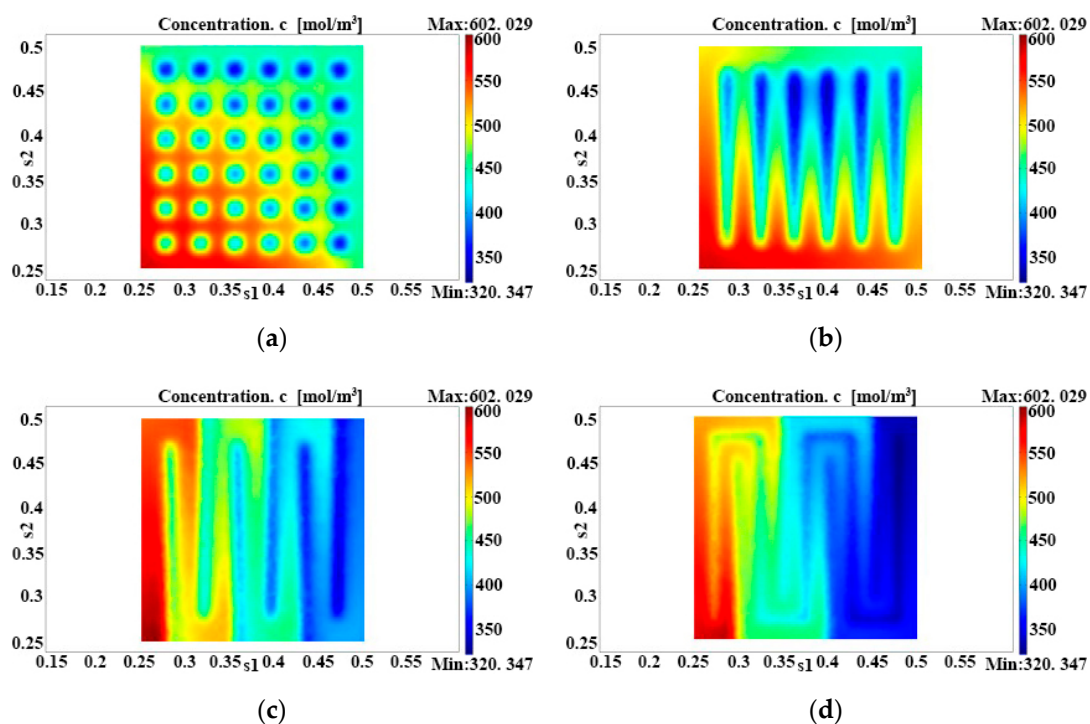


Figure 4. Methanol concentration distributions at the catalyst layers under (a) grid flow fields, (b) parallel flow fields, (c) single-serpentine flow fields, and (d) double-serpentine flow fields.

By solving Equation (12) in the model, we conclude that the highest current densities in the catalyst layer of single-serpentine, double-serpentine, grid and parallel flow fields were 2910.11, 2903.72, 2986.76 and 2931.67 A/m², respectively. Clearly, the single-serpentine flow field was the best in that case. Compared with the other three flow fields, the single-serpentine flow field could guarantee the uniform distributions and high-efficiency mass transport of anode reactants as well as the effective discharge of the products; all of these advantages made the single-serpentine flow field best fit the anode of μ DMFCs.

3.2. Different Open Ratios of Single-Serpentine Flow Fields

Figure 5 illustrates the methanol concentration distributions in the single-serpentine anode flow fields with four different open ratios, and the inlet methanol concentrations all set as 1000 mol/m³. It is clearly seen that the methanol concentration in the single-serpentine flow field with an open ratio of 73.0% is the largest, with a difference of more than 300 mol/m³ between the concentration of the inlet and outlet. However, the dead mass transfer field at the bottom of the support ridge was most distinctive in the anode dif-

fusion layer, with an open ratio of 29.1% under the lowest concentration of 219.96 mol/m³. In addition, it was likely to cause the concentration polarization. With the same single-serpentine flow field, we concluded that the wide support ridge could result in the dead mass transport field of reactants, which makes the methanol mass transport hard in the diffusion layer under the ridge. On the other hand, the methanol concentration distributions would be not uniform with a narrow support ridge, and they would also reduce the cell performance. Therefore, we found the best open ratio for anode flow fields to balance the cons and pros. As shown in Figure 5, methanol concentration distributions in anode flow fields were more uniform when the open ratio was 47.3% and 60.6%, and it was in favor of the stability of μ DMFCs.

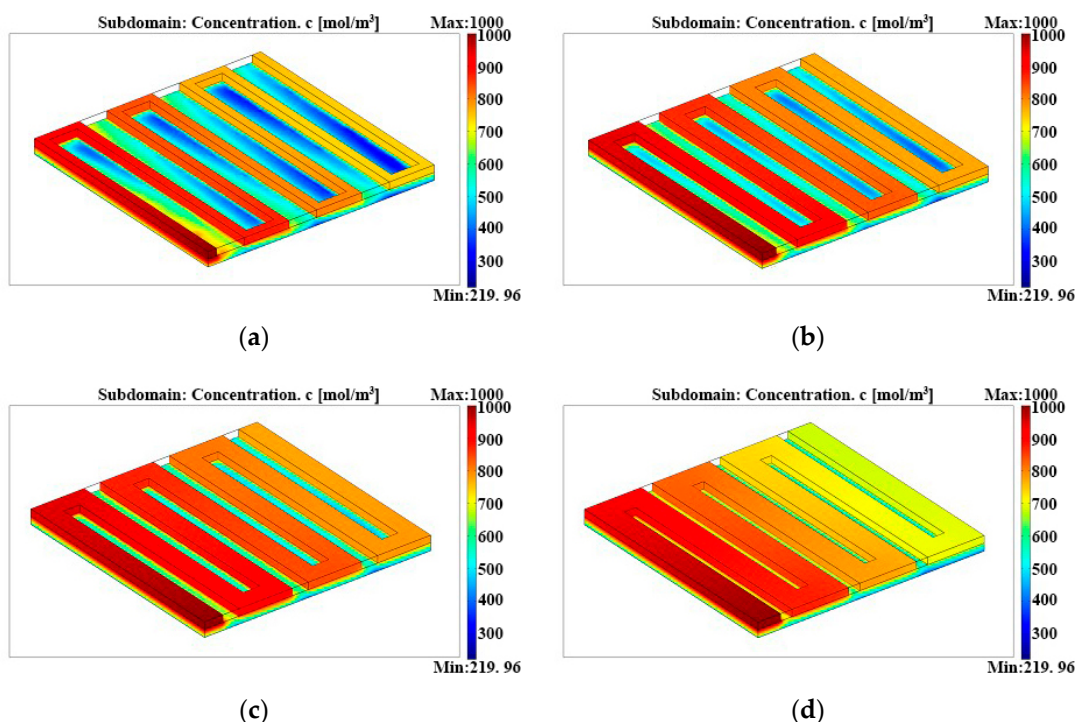


Figure 5. Methanol concentration distributions in the anode single-serpentine flow fields with different open ratios: (a) open ratio = 29.1%, (b) open ratio = 47.3%, (c) open ratio = 60.6%, and (d) open ratio = 73.0%.

Figure 6 shows the current density distributions at the catalyst layers along the x direction under the conditions of different open ratios. According to Figure 6, we could observe that the current density at $x = 0$ with an open ratio of 29.1% was the highest with a value of 3068.12 A/m². However, the current density at $x = 0.008$ with the same open ratio was the lowest (only 1263.97 A/m²). Comparatively, the current densities were more uniform with open ratios of 60.6% and 73.0%. Therefore, it was favorable to increase the utilizations of reactants and catalysts, while it was not easy to have the concentration polarization.

3.3. Different Channel Lengths of Single-Serpentine Flow Fields

Figure 7 shows the pressure distributions in the serpentine flow fields with different channel lengths. As shown in Figure 7, the pressure difference of the inlet and outlet increase gradually with the increment of channel lengths. Based on the above discussion, the pressure drop in the flow channels would contribute to the liquid flow, mass transfer of reactants and discharge of products. Therefore, the channel length of 96.03 mm could help the fuel cell achieve the best performance. However, the channel width would be reduced accordingly with an increment of the channel length. For instance, the channel with a length of 96.03 mm could only be 0.33 mm wide. In this way, the anode products

CO₂ blocking the channel will become larger, which not only brings about a decrease of the performance of the fuel cell but also increases the power loss of the external device for liquid feeding.

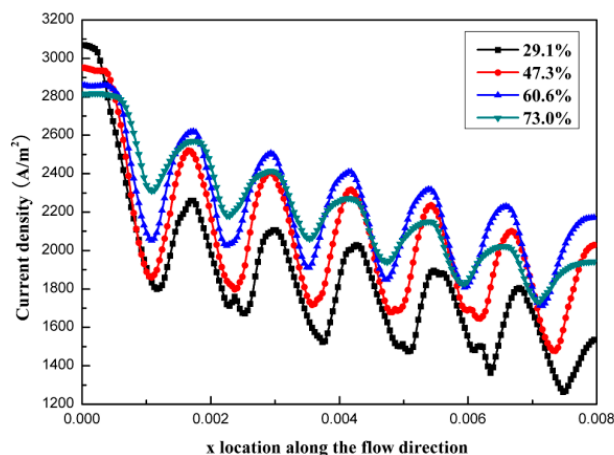


Figure 6. Current density distributions at the catalyst layers along the x direction under the conditions of different open ratios.

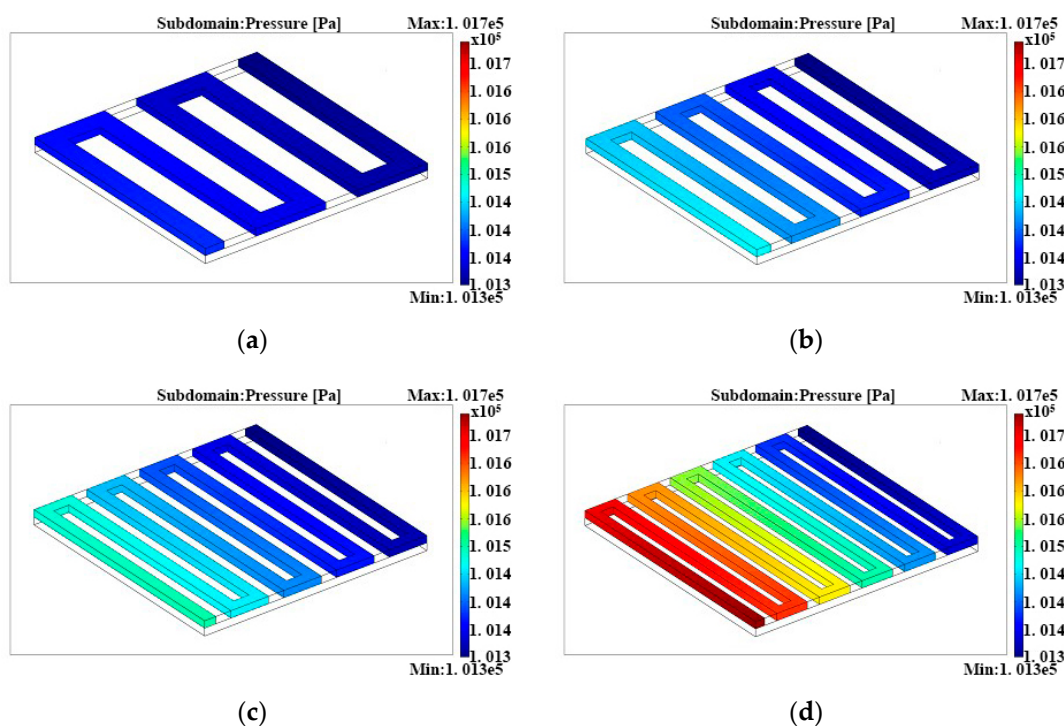


Figure 7. Pressure distributions in the anode serpentine flow fields with different channel lengths: (a) channel length = 47.32 mm, (b) channel length = 63.50 mm, (c) channel length = 79.60 mm, and (d) channel length = 96.03 mm.

Figure 8 shows methanol concentration distributions in the μ DMFCs anode flow fields with different channel lengths. With the increment of channel length, the methanol concentration difference between the inlet and outlet increases. Specifically, methanol concentration in the outlet with a length of 96.03 mm is around 150 mol/m³ lower than that with a length of 47.32 mm, and might decrease the mass transport efficiency in the outlet of the flow field. On the other hand, increasing the flow field length can improve the methanol mass transport in the diffusion layer. The diffusion dead area under the

support ridge can be decreased by increasing the pressure drop, and so the concentration polarization is reduced to a certain extent. Figure 9 shows the current density distributions at the catalyst layers along the x direction ($y = 0.004$) under the conditions of different channel length. The current density distributions are uneven with the channel length of 47.32 mm. The local current corresponding to the support ridge decreases sharply because this area could have low methanol concentrations. If the over-potential was increased, concentration polarization could occur due to a shortage of fuel. Furthermore, the current density distributions are even, with lengths of 79.60 and 96.03 mm. Though fluctuating a little, the current density average with the channel length of 63.5 mm is higher than the other three.

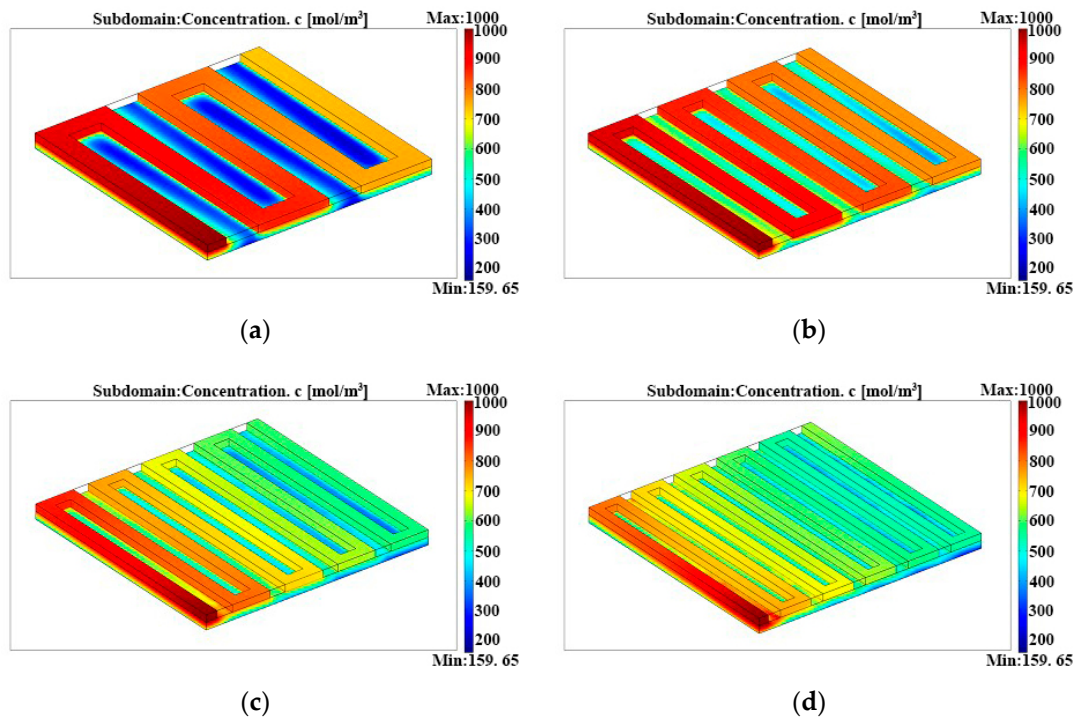


Figure 8. Methanol concentration distributions in the anode serpentine flow fields with different channel lengths: (a) channel length = 47.32 mm, (b) channel length = 63.50 mm, (c) channel length = 79.60 mm, and (d) channel length = 96.03 mm.

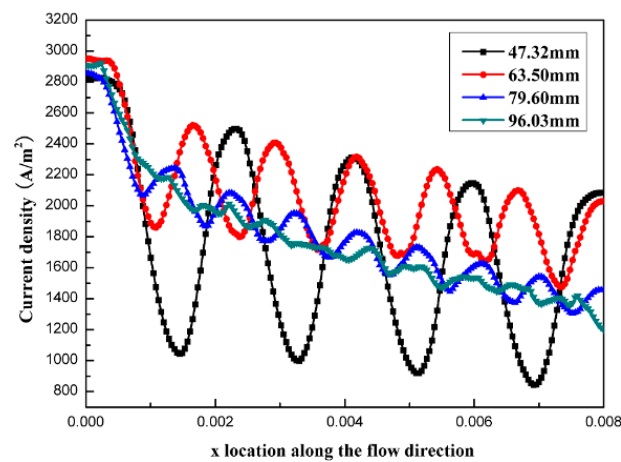


Figure 9. Current density distributions at the catalyst layers along the x direction under the conditions of different open ratios.

4. Experimental Verification

4.1. Fabrication and Assembly

In order to verify the accuracy of the simulation results, μ DMFCs with different flow fields were fabricated and assembled. Anode flow field configurations are summarized in Table 5. These configurations are the same as those used in the simulation shown in Section 2.1 Flow Field Design.

Table 5. Summary of the experimental anode flow field configurations.

| Type of Flow Field | Channel Width (mm) | Channel Depth (mm) | Channel Length (mm) | Ridge Width (mm) | Effective Area (mm × mm) | Open Ratio (%) |
|------------------------------|--------------------|--------------------|---------------------|------------------|--------------------------|----------------|
| Grid flow field | 0.55 | 0.24 | - ¹ | 0.69 | 7.99 × 7.99 | 72.9 |
| Parallel flow field | 0.75 | 0.24 | - ¹ | 0.45 | 7.95 × 7.95 | 72.9 |
| Single-serpentine flow field | 0.8 | 0.24 | 63.20 | 0.4 | 8.0 × 8.0 | 73.0 |
| Double-serpentine flow field | 0.575 | 0.24 | 43.30 ² | 0.25 | 8.0 × 8.0 | 73.6 |
| Single-serpentine flow field | 0.3 | 0.24 | 63.68 | 0.98 | 7.98 × 7.98 | 29.1 |
| | 0.5 | 0.24 | 63.50 | 0.75 | 8.0 × 8.0 | 47.3 |
| | 0.65 | 0.24 | 63.32 | 0.57 | 7.97 × 7.97 | 60.6 |
| | 0.8 | 0.24 | 63.20 | 0.4 | 8.0 × 8.0 | 73.0 |
| Single-serpentine flow field | 0.68 | 0.24 | 47.32 | 1.15 | 8.0 × 8.0 | 47.4 |
| | 0.5 | 0.24 | 63.50 | 0.75 | 8.0 × 8.0 | 47.3 |
| | 0.4 | 0.24 | 79.60 | 0.55 | 8.0 × 8.0 | 47.8 |
| | 0.33 | 0.24 | 96.03 | 0.44 | 8.03 × 8.03 | 47.5 |

¹ The channel length is meaningless in grid flow field and parallel flow field. ² The channel length of the double-serpentine flow field given is the length of a single channel.

A 5-layer MEA with an active area of 0.8 cm × 0.8 cm was fabricated using GDL hot pressing on both sides of the CCM at 130 °C and 4 MPa for 120 s. The 4.0 mgcm⁻² Pt-Ru anode catalyst, 4.0 mgcm⁻² Pt cathode catalyst, and Nafion117 membrane as a proton exchange membrane were used to manufacture the CCM by the decal transfer method. The gas diffusion layer (GDL) is carbon paper (TGPH-090, Toray Inc., Tokyo, Japan), which was prepared with the hydrophobic (10 wt.% PTFE for the anode and 30 wt.% PTFE for the cathode) and pore-formed (NH₄HCO₃) pretreatment.

The 480 ± 10 μm crystal silicon <100> crystal orientation was used to fabricate the current collector with different patterns using bulk-silicon MEMS technology. First, a 0.8-μm-thick Si₃N₄ layer was deposited on a silicon wafer by low pressure vapor deposition. The anode microchannel pattern was formed on the layer by photolithography. Then, the 240 μm deep channels were etched using an anisotropic etching process of 40% KOH at 40 °C. In order to realize a self-breathing cathode, a perforated silicon wafer with a uniform diameter of 0.6 mm was prepared as the cathode. A Ti/Au (0.05 μm/1.0 μm) layer was sputtered on the surface of the current collector to improve current collection and reduce contact resistance.

The MEA was sandwiched between the anode and cathode current collector to form a micro self-breathing direct methanol fuel cell. A clear adhesive was used to complete the seal. The assembly picture is shown in Figure 10. The experiment was carried out at room temperature and atmospheric pressure. A peristaltic pump was used to feed low concentration (1 M) methanol at a feeding rate of 1 mL min⁻¹. The performance was measured using an electronic load (N3300A&N3302A, Agilent Technologies, Santa Clara, CA, USA).

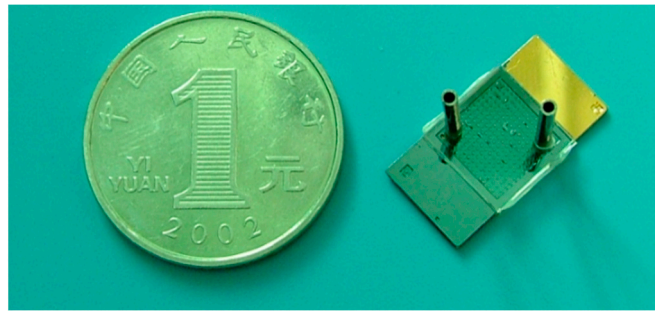


Figure 10. Photograph of an assembled self-breathing micro direct methanol fuel cell (μ DMFC).

4.2. Test

We first tested the performance of μ DMFCs with grid, parallel, single-serpentine and double-serpentine flow fields. The experiments were performed with dilute methanol (concentration 1 M) at the flow rate of 1 mL min^{-1} and at room temperature and atmospheric pressure. Figure 11 shows the performances of the μ DMFCs with different anode flow fields. Under different flow field conditions, the cell performance was obviously different, but there is a peak power density. Concentration polarization is the main cause of cell performance decline after peak power density. We found that the micro direct methanol fuel cell with a single-serpentine flow field obtained the best power density of 11.39 mW/cm^2 . However, grid and parallel flow fields showed an earlier power density drop. This indicated that different flow fields have a great influence on the concentration distribution and the single-serpentine flow field has uniform concentration distributions and better carbon dioxide removal. This is consistent with the simulation results.

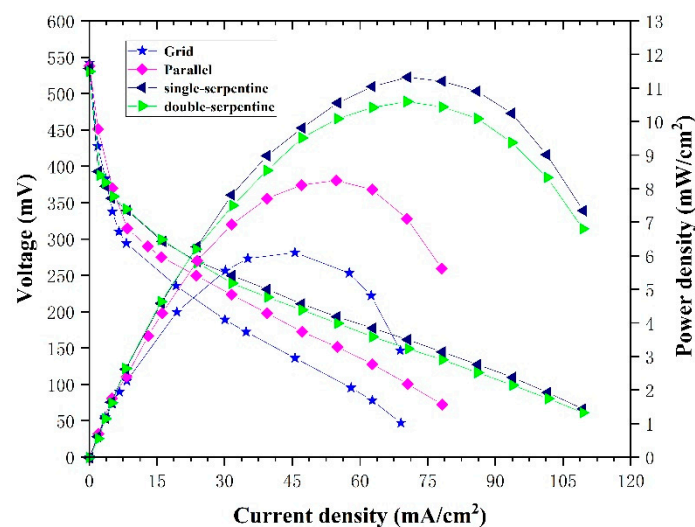


Figure 11. Polarization curves and power density curves of different flow fields under the same experimental conditions.

From the simulation results for single-serpentine flow fields of different open ratios, it seems that the best performance should be obtained with a 60.6% opening ratio. However, the experimental results in Figure 12 show that the performance decreases in the order of 47.3%, 60.6%, 73.0% and 29.1%, and the maximum power densities are 16.83 , 15.13 , 11.39 and 10.83 mWcm^{-2} , respectively. This seems to differ from the simulation results. In fact, under the condition of the same channel length, the opening ratio determined the channel width. A wider flow channel size will improve the mass transfer between methanol and the diffusion layer, and improve the removal of carbon dioxide. However, an excessively wide channel reduces the width of the rib and increases the contact resistance

and methanol crossover. Therefore, due to a channel wider than 29.1% and narrower than 60.6% and 73.0%, the opening ratio of 47.3% achieved the best performance. For a better evaluation of the influence of open ratios on cell performance, we tested the single cell electrochemical impedance spectroscopy (EIS) at a current of 30 mA, with the frequency from 60 kHz to 100 Hz and 10 mV amplitude, as shown in Figure 13. It can be seen that the internal resistance decreases in the order of 47.3%, 60.6%, 73.0% and 29.1%, and was 0.529, 0.587, 0.728 and 0.781 ohm, respectively, which justified the analysis above.

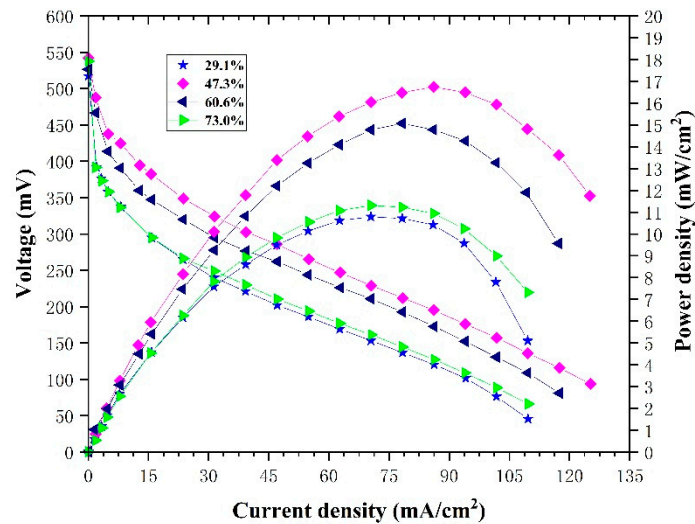


Figure 12. Polarization curves and power density curves of single-serpentine flow fields with different open ratios under the same experimental conditions.

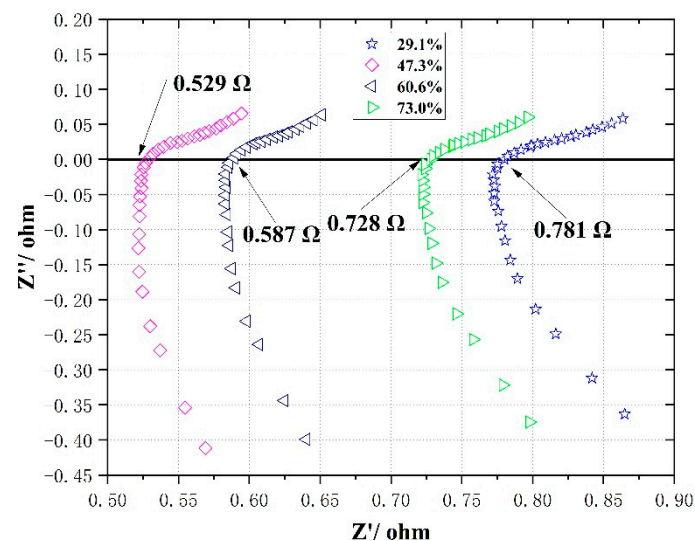


Figure 13. Nyquist plots of single-serpentine flow fields with different open ratios at high frequencies.

Figure 14 shows the performance of the μ DMFCs with different channel lengths at the same open ratio. The experimental results show that the best power density is 16.83 mWcm^{-2} with the length of 63.50 mm. The result is consistent with the simulation. If the length increases or decreases, the performance degrades. The main reason is that the different length of the channel causes a change of the width of the channel and the rib, resulting in a change of the μ DMFC performance.

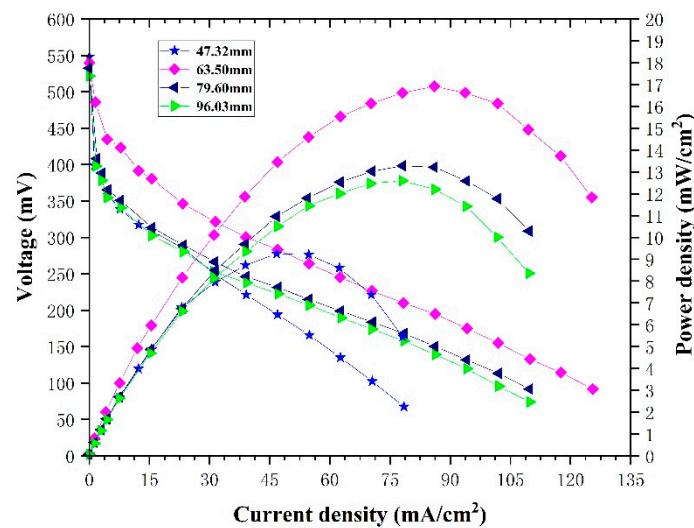


Figure 14. Polarization curves and power density curves of single-serpentine flow fields with different channel lengths under the same experimental conditions.

Through the above experiments and analysis, the optimal parameters of single-serpentine flow field were determined as 63.5 mm channel length and 47.3% open ratio. The durability of an air-breathing fuel cell with a single-serpentine flow field at optimal parameters was tested at a constant current density of 30, 60, and 90 mAcm^{-2} respectively. Figure 15 shows the voltage variations of the cell over 100 min. The voltage output of the cell at a constant current density of 90 mAcm^{-2} was more serious, which is mainly because of the fuel starvation at the back end of the cell.

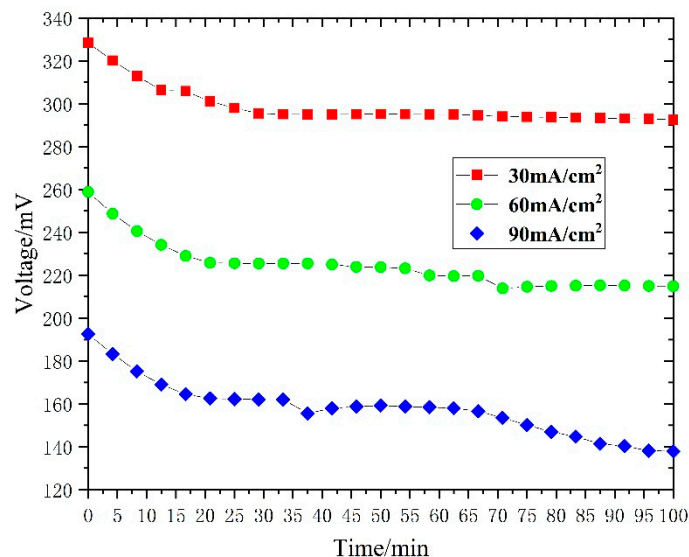


Figure 15. Durability testing results of an air-breathing fuel cell with a single-serpentine flow field at 63.5 mm channel length and 47.3% open ratio at a constant current density of 30, 60, and 90 mAcm^{-2} , respectively.

5. Conclusions

In this work, the influence of different anode flow fields on the performance of μDMFCs was analyzed by establishing a 3D model of the micro direct methanol fuel cell. A silicon-based direct methanol fuel cell was fabricated and assembled to verify the simulation results. The simulation and experimental results show that compared with grid, parallel and double-serpentine flow fields, the single-serpentine flow field could

guarantee uniform distributions and high-efficiency mass transport and the removal of carbon dioxide. In addition, the micro direct methanol fuel cell with a single-serpentine flow field produced a maximum power density of 16.83 mWcm^{-2} at room temperature and atmospheric pressure. For the serpentine flow field, the optimal open ratio of 47.3% and channel length of 63.50 mm were obtained.

Author Contributions: Conceptualization, H.D.; methodology, H.D. and Y.Z.; validation and investigation, H.D. and J.Z.; data curation, J.Z.; writing—review and editing, H.D. and J.Z. All authors have read and agreed to the published version of the manuscript.

Funding: This research was funded by National Natural Science Foundation of China, (No. 51975023).

Conflicts of Interest: The authors declare no conflict of interest.

References

1. Alias, M.; Kamarudin, S.; Zainoodin, A.; Masdar, M. Active direct methanol fuel cell: An overview. *Int. J. Hydrog. Energy* **2020**, *45*, 19620–19641. [[CrossRef](#)]
2. Xia, Z.; Zhang, X.; Sun, H.; Wang, S.; Sun, G. Recent advances in multi-scale design and construction of materials for direct methanol fuel cells. *Nano Energy* **2019**, *65*, 104048. [[CrossRef](#)]
3. Chen, X.; Li, T.; Shen, J.; Hu, Z. From structures, packaging to application: A system-level review for micro direct methanol fuel cell. *Renew. Sustain. Energy Rev.* **2017**, *80*, 669–678. [[CrossRef](#)]
4. Munjewar, S.S.; Thombre, S.B.; Mallick, R.K. A comprehensive review on recent material development of passive direct methanol fuel cell. *Ionics* **2016**, *23*, 1–18. [[CrossRef](#)]
5. Falcao, D.S.; Oliveira, V.B.; Rangel, C.M.; Pinto, A.M.F.R. Review on micro-direct methanol fuel cells. *Renew. Sustain. Energy Rev.* **2014**, *34*, 58–70. [[CrossRef](#)]
6. Kumar, P.; Dutta, K.; Das, S.; Kundu, P.P. An overview of unsolved deficiencies of direct methanol fuel cell technology: Factors and parameters affecting its widespread use. *Int. J. Energy Res.* **2014**, *38*, 1367–1390. [[CrossRef](#)]
7. Chen, X.; Zhang, Z.; Shen, J.; Hu, Z. Micro direct methanol fuel cell: Functional components, supplies management, packaging technology and application. *Int. J. Energy Res.* **2017**, *41*, 613–627. [[CrossRef](#)]
8. Mallick, R.K.; Thombre, S.B.; Shrivastava, N.K. A critical review of the current collector for passive direct methanol fuel cells. *J. Power Sources* **2015**, *285*, 510–529. [[CrossRef](#)]
9. Wang, L.; Yin, L.; Yang, W.; Cheng, Y.; Feng, X. Evaluation of structural aspects and operation environments on the performance of passive micro direct methanol fuel cell. *Int. J. Hydrog. Energy* **2020**, *46*, 2594–2605. [[CrossRef](#)]
10. Braz, B.A.; Moreira, C.S.; Oliveira, V.B.; Pinto, A.M.F.R. Effect of the current collector design on the performance of a passive direct methanol fuel cell. *Electrochim. Acta* **2019**, *300*, 306–315. [[CrossRef](#)]
11. Yuan, Z.; Yang, J.; Li, X.; Wang, S. The micro-scale analysis of the micro direct methanol fuel cell. *Energy* **2016**, *100*, 10–17. [[CrossRef](#)]
12. Rao, A.S.; Rashmi, K.R.; Manjunatha, D.V.; Jayarama, A.; Pinto, R. Enhancement of power output in passive micro direct methanol fuel cells with optimized methanol concentration and trapezoidal flow channels. *J. Micromech. Microeng.* **2019**, *29*, 075006. [[CrossRef](#)]
13. Hu, X.Q.; Yang, Q.W.; Xiao, G.; Chen, X.T.; Qiu, X. Power generation enhancement in direct methanol fuel cells using non-uniform cross-sectional serpentine channels. *Energy Convers. Manag.* **2019**, *188*, 438–446. [[CrossRef](#)]
14. El-Zoheiry, R.M.; Ookawara, S.; Ahmed, M. Efficient fuel utilization by enhancing the under-rib mass transport using new serpentine flow field designs of direct methanol fuel cells. *Energy Convers. Manag.* **2017**, *144*, 88–103. [[CrossRef](#)]
15. Chen, W.; Yuan, W.; Ye, G.; Han, F.; Tang, Y. Utilization and positive effects of produced CO₂ on the performance of a passive direct methanol fuel cell with a composite anode structure. *Int. J. Hydrog. Energy* **2017**, *42*, 15613–15622. [[CrossRef](#)]
16. Liang, J.; Liu, K.; Li, S.; Wang, D.; Ren, T.; Xu, X.; Luo, Y. Novel Flow Field with Superhydrophobic Gas Channels Prepared by One-step Solvent-induced Crystallization for Micro Direct Methanol Fuel Cell. *Nano-Micro Lett.* **2015**, *7*, 165–171. [[CrossRef](#)]
17. Yan, X.H.; Zhao, T.S.; An, L.; Zhao, G.; Zeng, L. A micro-porous current collector enabling passive direct methanol fuel cells to operate with highly concentrated fuel—ScienceDirect. *Electrochim. Acta* **2014**, *139*, 7–12. [[CrossRef](#)]
18. Ouellette, D.; Ozden, A.; Ercelik, M.; Colpan, C.O.; Ganjehsarabi, H.; Li, X.; Hamdullahpur, F. Assessment of different bio-inspired flow fields for direct methanol fuel cells through 3D modeling and experimental studies. *Int. J. Hydrog. Energy* **2017**, *43*, 1152–1170. [[CrossRef](#)]
19. Ozden, A.; Ercelik, M.; Ouellette, D.; Colpan, C.O.; Ganjehsarabi, H.; Hamdullahpur, F. Designing, modeling and performance investigation of bio-inspired flow field based DMFCs. *Int. J. Hydrog. Energy* **2017**, *42*, 21546–21558. [[CrossRef](#)]